The Journal of Experimental Biology 211, 274-279
Published by The Company of Biologists 2008
doi:10.1242/jeb.012849

Research article

Propulsive performance of biologically inspired flapping foils at high Reynolds numbers

Alexandra H. Techet
Massachusetts Institute of Technology, Department of Mechanical Engineering, Cambridge, MA 02139, USA
e-mail: ahtechet@mit.edu

Accepted 24 September 2007

Summary

Propulsion and maneuvering underwater by flapping foil motion, optimized through years of evolution, is ubiquitous in nature, yet marine propulsors inspired by examples of highly maneuverable marine life or aquatic birds are not widely implemented in engineering. Performance data from flapping foils, moving in a rolling and pitching motion, are presented at high Reynolds numbers, Re=Uc/ν, or O(10^4), where U is the relative inflow velocity, c is the chord length of the foil, and ν is the kinematic viscosity of the fluid, from water tunnel experiments using a foil actuator module designed after an aquatic penguin or turtle fin. The average thrust coefficients and efficiency measurements are recorded over a range of kinematic flapping amplitudes and frequencies. Results reveal a maximum thrust coefficient of 2.09, and for low values of angle of attack the thrust generally increases with Strouhal number, without much penalty to efficiency. Strouhal number is defined as $St=2h_0f/U$, where f is the frequency of flapping, and $2h_0$ is the peak-to-peak amplitude of flapping. The thrust and efficiency contour plots also present a useful performance trend where, at low angles of attack, high thrust and efficiency can be gained at sufficiently high Strouhal numbers. Understanding the motion of aquatic penguins and turtle wings and emulating these motions mechanically can yield insight into the hydrodynamics of how these animals swim and also improve performance of biologically inspired propulsive devices.

Key words: fish swmming, flapping foil, propulsion, hydrodynamics.

Introduction

The design of biologically inspired propulsion mechanisms for underwater vehicles continues to generate significant interest in the hydrodynamics of fish swimming. Fish and animals, such as aquatic penguins and turtles, are highly adapted to swimming in the ocean and serve as excellent models for developing novel propulsive devices for underwater vehicles. With the goal of designing compact, agile autonomous and unmanned underwater vehicles (AUVs and UUVs), engineers have turned to fish and their aquatic counterparts for inspiration (e.g. Bandyopadhyay, 2005; Anderson and Chabra, 2002; Triantafyllou et al., 2000; Anderson et al., 1998; Bandyopadhyay et al., 1997). Biologists have studied the kinematics and morphology of swimming fish in great detail, revealing the superior agility of these creatures (e.g. Fish and Lauder, 2006; Lauder, 2000; Drucker and Lauder, 1999; Videler, 1993; Fish and Hui, 1991). The undulatory nature of the fish body motion imparts flow control on the surrounding fluid generating a unique propulsive signature in the form of a reverse Kármán vortex street (Triantafyllou and Triantafyllou, 1995). This simplified view of the wake structure does not account for three-dimensional effects that result from the geometry of the fish body and tail fin.

Flapping foils have been used as models for swimming fish fins to better understand fish swimming hydrodynamics. Heaving and pitching foils with moderate to high aspect ratios (Anderson, 1996; Triantafyllou et al., 1993), and more three-dimensional motions of foils, modeling pectoral fins with lower aspect ratios, have also been investigated as alternative methods of propulsion for underwater vehicle technology (Bandyopadhyay, 2005; Lang et al., 2006; Kato, 2000). Extensive studies of the two-dimensional wake patterns behind flapping foils and live and robotic swimming fish have been performed both experimentally and numerically. Thorough reviews of this research on flapping foils can be found in the literature (Triantafyllou et al., 2004; Triantafyllou el al., 2005).

Typical wake patterns generated by the two-dimensional flapping foil motion consist of alternately rotating vortices organized to form a jet-like wake, or reverse Kármán street, which results in thrust generation over a range of Strouhal numbers and kinematic parameters. Strouhal number is defined as $St=2h_0f/U$, where $2h_0$ is the peak-to-peak heave amplitude of the trailing edge, f is the flapping frequency (in Hz), and U is the incoming flow velocity relative to the foil. Optimal propulsive performance has been shown to be highly dependent on Strouhal number. Typically, flapping foils used for propulsion have high efficiencies in a range of Strouhal numbers 0.2–0.4 (Triantafyllou and Triantafyllou, 1995); higher thrust values can be achieved at higher values of Strouhal number but with less efficiency.

The unsteady flapping motion of a foil generates vorticity at the trailing edge and tips of the foil and also at the leading edge under certain conditions. These patterns vary with the amplitude and frequency of the motion as well as the shape of the kinematics employed (e.g. Hover et al., 2004; Anderson el al., 1998; Koochesfahani, 1989; Katz and Weihs, 1979). Experiments with heaving and pitching symmetric foils, with a maximum thickness that is 15% of the chord length (i.e. a NACA 0015 foil), at moderate Reynolds numbers [5000–12 000 (Freymouth, 1990)] link the

formation of a leading edge vortex, and its successive combination with the vorticity generated at the trailing edge, with high lift coefficients. Reynolds number (*Re*) is defined as the ratio of the inertial fluid forces to the viscous fluid forces: $Re=(\rho U^2 c^{-1})/(\mu U c^{-2})=\rho U c/\mu$, where ρ is the density of the fluid, and μ the dynamic viscosity of the fluid. *Re* is often written in terms of kinematic viscosity: $\nu=\mu/\rho$; for water $\nu=10^{-6}$ m^2 s^{-1}. This interaction is also important to achieve high efficiency for flapping foil swimming modes (Anderson et al., 1998).

A closer look at performance of finite aspect ratio, three-dimensional flapping foils is warranted at higher Reynolds numbers, in order to design vehicles to swim with optimal kinematics and maximizing thrust while optimizing efficiency. In an effort to understand this trade-off, tests were performed using a three-dimensional, linearly tapered hydrofoil forced to move in roll and pitching motions, and the measured force and hydrodynamic efficiency data are presented, discussed and compared with data reported from previous tests (Flores, 2003; McLetchie, 2004; Polidoro, 2003; Read, 2000).

Experimental methods

Three-dimensional flapping foil apparatus and kinematics

The three-dimensional (3D) flapping foil motion emulates that of an aquatic penguin wing or turtle fin. The 3D flapping foil actuator was constructed as a dual-canister design: two watertight canisters, one each for pitch and roll, house the motor and chain drive for each motion separately. The two canisters are coupled together and to the foil (see Fig. 1A). This apparatus is mounted in the Massachusetts Institute of Technology recirculating water tunnel, capable of flow speeds from 0.5 to 5.0 m s^{-1} with turbulence levels under 3%. The tunnel's square test section is 0.5 m×0.5 m×1.25 m long. Constrained to move in roll $\phi(t)$ and pitch $\theta(t)$ only, a diagram of the motion coordinate system is given in Fig. 1B. This type of flapping apparatus presents underwater vehicle designers and engineers a simpler design problem, e.g. fewer sealing issues, than the heaving/pitching foil. The thesis by Lim (Lim, 2005) presents further details of the housing design and operation.

The kinematic motion of the foil is measured through potentiometers mounted to each rotating shaft, which map the pitch and roll motion, and also through the encoders mounted on each motor. The encoder data are used for redundancy and kinematics validation. A torque sensor is coupled to the roll motor shaft to calculate the power input from the motor end during actuation; the power input can be used to determine the mechanical efficiency of the flapping foil. The forces and torques acting directly on the foil are measured with a six-axis, waterproof strain gauge sensor, which measures the three force components (F_x, F_y, F_z) and the three moment components (M_x, M_y, M_z). Hydrodynamic efficiency is calculated using the torque measurements from the six-axis sensor to calculate power input to the fluid by the foil, thus bypassing the mechanical losses in the drive mechanism. Cross-coupling between the six channels is eliminated using the factory supplied matrix, which has been validated extensively (Lim, 2005).

The average thrust and lift forces are found by applying a force rotation matrix to the force traces and averaging the data over 10–15 cycles. Average force data presented in subsequent sections are given in terms of the non-dimensional force coefficient, based on the planform area of the foil, instead of the swept area as would be used for a propeller. The hydrodynamic efficiency is determined by comparing the power output, calculated from the product of average thrust and velocity, to the sum of the power input, applied to the pitch and roll axes.

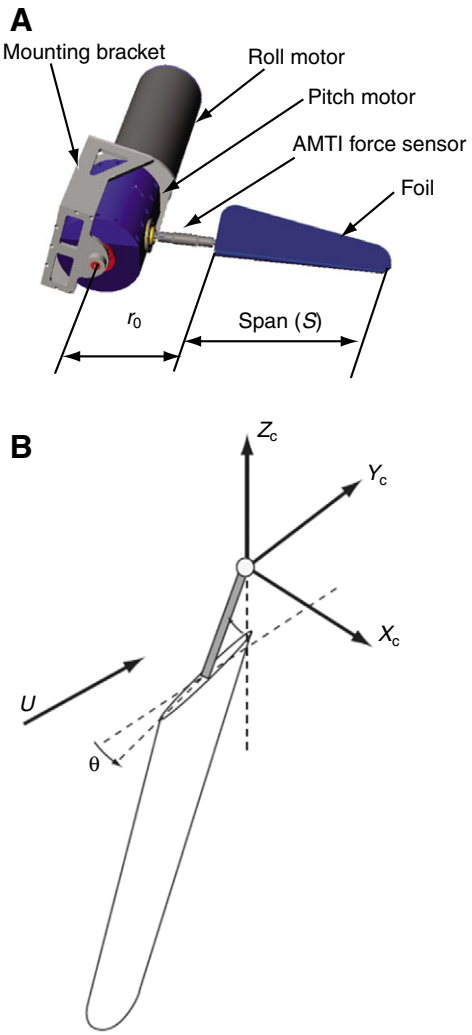

Fig. 1. (A) Double canister flapping foil actuator design with the foil and the inline AMTI six-axis force sensor assembly between the pitch canister and the foil. The distance from center of roll axis to root of foil is indicated by r_0; S is the foil span. (B) Foil motion coordinate system. The freestream flow is in the Y_c direction and Z_c is oriented in the opposite direction from gravity. Roll, $\phi(t)$, is constrained to the X_c–Z_c plane and pitch, $\theta(t)$, is an angular motion about the foil shaft.

The prescribed roll and pitch motions are simple sinusoidal harmonics with the same circular frequency ω (rad s^{-1}). The roll motion of the foil is given by:

$$\phi(t) = \phi_0 \sin(\omega t) , \quad (1)$$

where ϕ_0 is the roll amplitude in radians; the pitch motion of the foil is defined as:

$$\theta(t) = \theta_0 \sin(\omega t + c) + \theta_{bias} , \quad (2)$$

where θ_0 is the pitch amplitude and ψ is the phase angle between pitch and roll, both in radians. The static pitch bias θ_{bias} is an optional parameter that introduces a non-zero average pitch angle to the foil; for these tests it is set to zero. The phase angle ψ for the tests is set to $\pi/2$, as recommended (Read et al., 2003).

The angle of attack profile varies along the span of the three-dimensional flapping foil as it rolls and pitches. To simplify the kinematics, the motion can be decomposed to 2D heaving and pitching, *versus* rolling and pitching, at any span location on the

foil. Although McLetchie's results (McLetchie, 2004) show varying centers of force, the 70% span location is selected to be consistent with conventional propeller notations and for easy comparison with past flapping foils experiments. This location is defined as:

$$r_{0.7} = r_0 + 0.7S\,, \tag{3}$$

where r_0 is the distance from the center of roll axis to the root of the foil, and S is the span of the foil, as shown in Fig. 1A. The heave position is defined as:

$$h(t) = h_0 \sin(\omega t)\,, \tag{4}$$

where h_0 is the amplitude of the heave motion at $r_{0.7}$; h_0 is defined as:

$$h_0 = r_{0.7}\phi_0\,. \tag{5}$$

The angle of attack at one span location can be found from the instantaneous pitch position of the foil and the ratio of the heave to forward velocity. Fig. 2 shows the vector diagram of the velocity components.

The true angle of attack profile can be calculated mathematically. Since a foil with a positive pitch produces a smaller angle of attack, one needs to subtract the angle of attack due to pitch from that due to roll to find the overall angle of attack profile:

$$\alpha(t) = \arctan\left(\frac{\dot{h}\,(t)}{U}\right) - \theta(t)\,, \tag{6}$$

where U is the forward speed of the actuator and $\dot{h}$ is the heave velocity. From Eqn 4, we can express the heave velocity as:

$$\dot{h}(t) = \omega r_{0.7}\phi_0 \cos(\omega t)\,. \tag{7}$$

Substituting Eqn 7 into Eqn 6, we get the expression for angle of attack in 3D kinematics:

$$\alpha(t) = \arctan\left(\frac{\omega r_{0.7}\phi_0 \cos(\omega t)}{U}\right) - \theta_0 \cos(\omega t) - \theta_{\text{bias}}\,. \tag{8}$$

The maximum angle of attack, $\alpha_{\max}$, is calculated using Eqn 8 at $r_{0.7}$; $\alpha_{\max}$ is given in degrees throughout this paper.

Again, the Strouhal number can be used to describe the foil motion kinematics based on the roll amplitude and $r_{0.7}$:

$$St = \frac{2h_0 f}{U} = \frac{2r_{0.7}\phi_0 f}{U}\,. \tag{9}$$

An estimate of the total width of the wake produced by the flapping foil is $2h_0$. This is essentially the peak-to-peak amplitude of the foil taken at the 0.7 chord for a 90° phase offset between heave and pitch. The roll amplitude is non-dimensionalized by converting this to 2D heave amplitude at 0.7 span and dividing by the chord length, $h_{0.7}/c$. Finally, Reynolds number, $Re = Uc_{0.7}/\nu$, is calculated based on the chord at 70% of the span, $c_{0.7}$, and kinematic viscosity of the fluid, $\nu = 10^{-6}$ m^2 s^{-1}.

The foil used in this experiment is fabricated with a NACA 0012 cross section. The NACA 0012 is a standard, symmetric foil profile with a maximum thickness that is 12% of the chord length (Abbott and von Doenhoff, 1959). The test foil has a span of 24.6 cm from root to tip, and an average chord length, $\bar{c}$, of 5.5 cm from leading edge to trailing edge. The foil has a linearly tapering trailing edge profile. Tests were performed over a range of kinematic parameters: heave/chord ratio, $h_{0.7}/c$={1.0, 1.5, 2.0}; Strouhal number, St={0.2:0.1:0.6}; and maximum angle of attack, $\alpha_{\max}$={15:5:45}°. The experiments were conducted at Reynolds numbers 27 000 to 55 000. The lower speed was used to achieve higher Strouhal numbers. The speed was monitored at all times by a Laser Doppler Velocimetry system and maintained to within ±0.01 m s^{-1}.

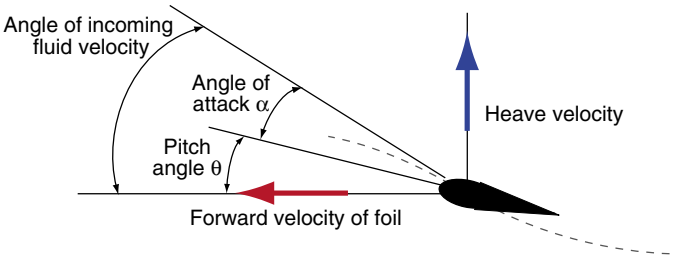

Fig. 2. Vector diagram for velocity components relative to heaving and pitching motions and incoming fluid velocity.

Results and Discussion

Three-dimensional flapping foil performance

The 3D flapping foil motion (roll/pitch) presents underwater vehicle designers with a more straightforward design problem compared to the heaving/pitching mechanism design and yields further insight into the performance of swimming animals such as aquatic penguins and turtles. To evaluate the performance of flapping foils sufficiently, accurate force and efficiency measurements are paramount. Force data are presented here for the 3D flapping foil mechanism for induced 2D heave-to-chord ratios (Eqn 4) $h_{0.7}/c$=1.0, 1.5 and 2.0, over a range of $\alpha_{\max}$ from 15° to 45°. Typical force traces obtained by the six-axis force sensor are presented in Fig. 3.

Using data acquired with the six-axis sensor, the average thrust of the foil is calculated by:

$$\bar{F}_{x_0} = \frac{1}{T}\int_0^T \bar{F}_{x_0}(t)\mathrm{d}t\,. \tag{10}$$

$\bar{F}_{x_0}$ is the x-force component translated into the reference frame of the tunnel, averaged over one flapping cycle. By axes convention, x is positive upstream. A non-dimensional thrust coefficient can be defined as:

$$C_{\mathrm{T}} = \frac{-2\bar{F}_{x_0}}{\rho U^2 \bar{c} S}\,, \tag{11}$$

where ρ is the fluid density, U is the relative flow velocity, S is the foil span and $\bar{c}$ is the average chord length.

The general trend of the thrust results (Fig. 4) compares well with those for the 2D case (Read, 2000) and 3D case (McLetchie, 2004). The thrust coefficients decrease with decreasing Strouhal numbers and $\alpha_{\max}$ values, and increases with increasing values of both Strouhal number and $\alpha_{\max}$. At heave- to- chord ratio of 1.0 ($h_{0.7}/c$=1.0) a peak thrust coefficient of 1.6 is recorded at St=0.5 and $\alpha_{\max}$=30°. Extrapolating up to St=0.6, it appears that a higher peak thrust coefficient could be achieved. Such an increase is substantiated by McLetchie (McLetchie, 2004).

For the case of $h_{0.7}/c$=1.5, peak thrust coefficients were measured for St=0.6 and angle of attacks of 30° and 35°. At $h_{0.7}/c$=2.0, the

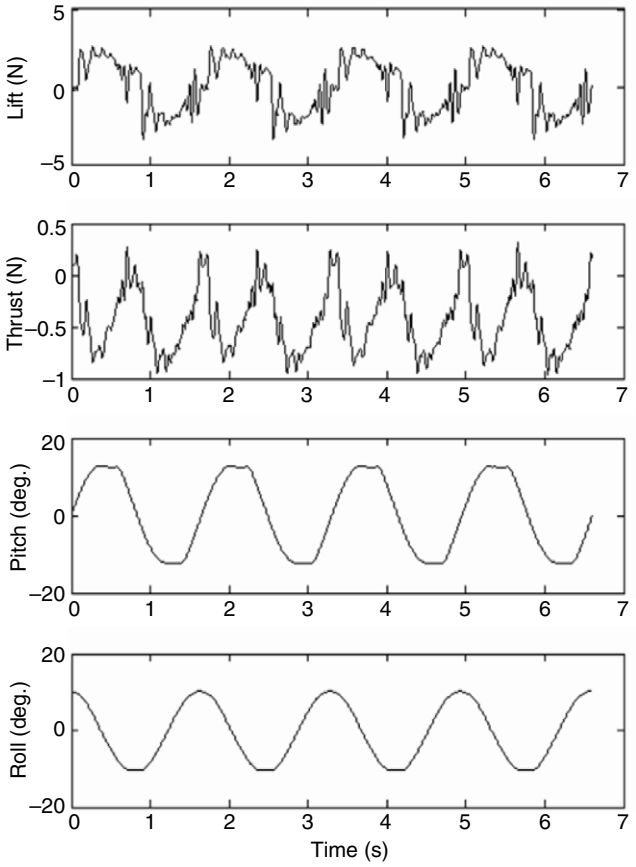

Fig. 3. Processed data recorded for St=0.2, $h_{0.7}/c$=1.5, α_{max}=20°. The horizontal axis is the time (in s). The lift and thrust are in the tunnel reference frame. The forces are calibrated using the AMTI sensitivity matrix.

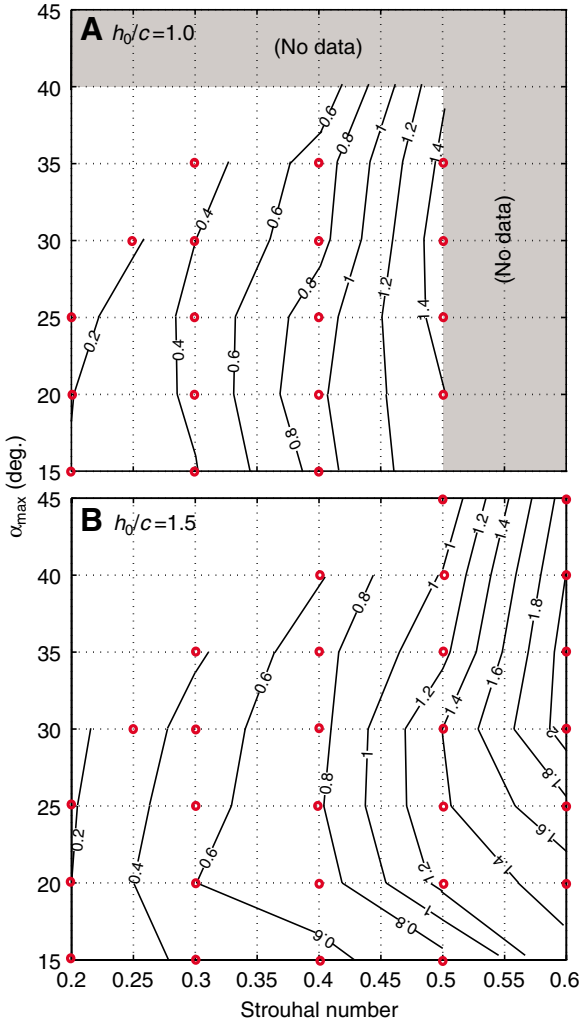

Fig. 4. Contour plots of thrust coefficient for h_0/c=1.0 (A) and h_0/c=1.5 (B); α_{max} is given in degrees. Red circles represent location of each run performed; no data exist for the region shadowed in grey for h_0/c=1.0.

maximum thrust coefficients now occur at the same Strouhal numbers (St=0.6) but have lower magnitudes at α_{max}=30° and 35° (Lim, 2005). Fig. 4 shows that for a given Strouhal number the thrust coefficient increases with the maximum angle of attack, but beyond a critical α_{max} value, the thrust coefficient is expected to decrease. This is similar to the data obtained for heaving/pitching foils at Re=750 and 1000 (Read, 2006). Increases in roll amplitude tend to have similar effects. The maximum thrust coefficient for these runs was recorded at $h_{0.7}/c$=1.5. At the higher roll amplitude, $h_{0.7}/c$=2.0, the peak thrust coefficient is lower, thus it is possible that an optimal roll amplitude can be found, between the heave-to-chord ratio of 1.5–2.0, for which the thrust coefficient can be maximized.

The left and bottom 'borders' of the parametric space represent the boundaries for which the angle of attack profiles tend to corrupt, i.e. some regions of the foil would encounter negative angles of attack, resulting in drag instead of thrust production. Here, the results at St=0.2 show very low thrust production for all α_{max} values. This low thrust boundary represent the transition in the wake from drag- to thrust-producing vortices (Flores, 2003). At high α_{max}, the transition to thrust does not occur until a Strouhal number of about 0.4. At experimental points for which low thrust values are measured ($St \leqslant 0.3$; $15° \leqslant \alpha_{max} \leqslant 25°$), there are large errors associated with the results (>10% in certain cases). A more thorough analysis of the error from these tests is given in Lim (Lim, 2005). In addition, the thrust coefficients presented above were evaluated based on planform area. A more appropriate normalization, in keeping with that used in propeller performance analysis, might have been to use the projected swept area. This formulation would have produced numerically smaller values of C_T (Techet el al., 2005).

The hydrodynamic efficiency of the foil is defined as the ratio of power output P_{out} over power input P_{in} to the fluid:

$$\eta = \frac{P_{out}}{P_{in}} . \quad (12)$$

Power output is the product of the time-averaged thrust and flow velocity:

$$P_{out} = TU = -\bar{F}_{x_0} U . \quad (13)$$

The power input P_{in} is the power input to the fluid, calculated from torque measurements with the six-axis sensor mounted to the foil shaft. While the torque sensor attached to the roll motor could measure the direct power input from the electric motor, a significant amount of the power is actually used to move the inertial mass of the pitch canister, and the losses due to backlash

in the motors can be quite large. The motor power input is found to be in the order of ten greater than the power transmitted to the flow. Thus a more useful approach is to use the power input measured by the AMTI sensor to calculate hydrodynamic efficiency of the foil, such that the hydrodynamic efficiency of the foil can be compared directly with other foil designs and aquatic animals in future research.

In a reverse fashion to the thrust coefficient results, efficiency peaks at the lower end of Strouhal and α_{max} values and then decreases with increasing *St* and α_{max} values (Fig. 5). This is as expected since, in low thrust regions, minimal energy is lost as a result of kinetic energy being imparted to the flow. The maximum efficiency recorded is about 0.7, centered at St=0.3 and α_{max}=20° for $h_{0.7}/c$=2.0. Its location corresponds with that reported by McLetchie (McLetchie, 2004), although the magnitudes of efficiency differ. Read also shares the same peak location with measured efficiencies not exceeding 0.7, for 2D flapping foils (Read, 2000).

Higher roll amplitudes result in greater energy expended in moving the foil through the large oscillations. It is only at higher frequencies where greater thrust is generated such that the efficiency appears to be improving. Figs 4 and 5 show that for low α_{max} values, thrust generally increases with Strouhal number without significant penalty to efficiency. This is good news with respect to designing mechanisms for underwater vehicles, as an optimal point can be identified for relatively high thrust production without sacrificing efficiency – it is also good news for aquatic swimmers, as they can produce significant propulsive forces with minimal effort. For example, at $h_{0.7}/c$=1.5, we see relatively high efficiencies occurring at St=0.5, and α_{max} of 15° and 20°. This offers a good design point where efficiencies of more than 0.6 can be achieved with thrust coefficients ranging from 0.7 to 1.2.

The average range of thrust coefficient C_T is found to be in the order of ±0.026, or ±0.044 N in terms of absolute thrust; as such, the percentage error, which is taken as the fraction of standard deviation over the mean, is naturally higher at the lower thrust runs (Lim, 2005). In the regions where the thrust is low ($St \leqslant 0.3$; $15° \leqslant \alpha_{max} \leqslant 25°$), the percentage errors associated with the measurements still remain significant and thus the efficiency measurements also require careful consideration and further validation. Likewise a larger percentage error for efficiency η also arises for these cases, since the error for η is a combination of errors from power input and thrust measurements.

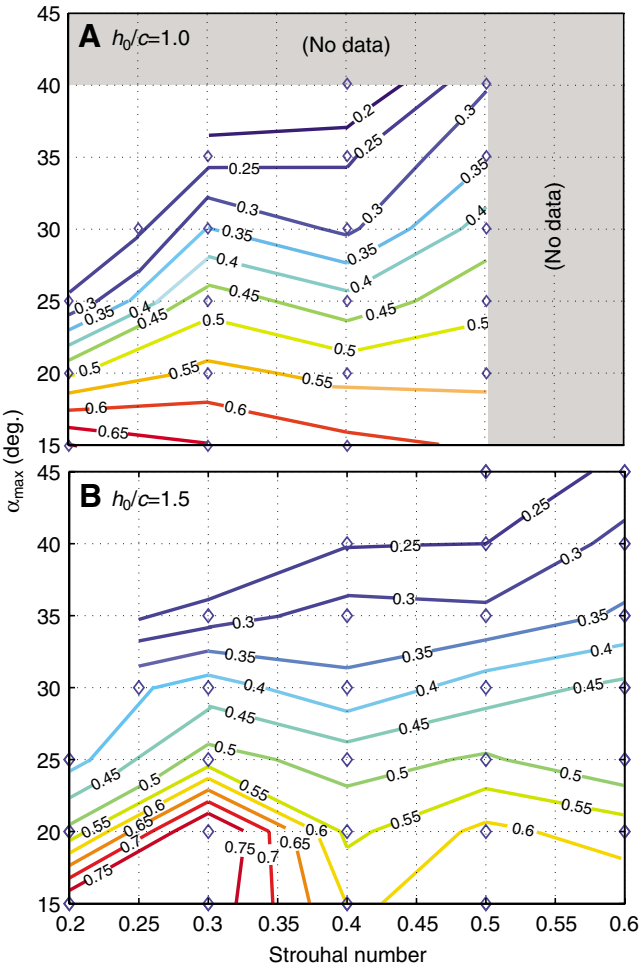

Fig. 5. Contour plots of thrust coefficient and efficiency for h_0/c=1.0 (A) and h_0/c=1.5 (B); α_{max} is given in degrees. Blue diamonds represent location of each run targeted; no data exist for the region shadowed in grey for h_0/c=1.0.

Conclusions

In summary, the 3D flapping foil, similar to a pectoral fin, holds the most promise for implementation in an underwater vehicle due to the reduced complexity over the heaving/pitching mechanism. To further extend our understanding of flapping foil performance at higher Reynolds numbers the 3D rolling/pitching foil apparatus was studied in a water tunnel at Reynolds numbers on the order of $Re \sim 10^4$. These tests, using force sensors to measure thrust and efficiency, with the 3D flapping foils are highly valuable from a design point of view.

Clearly indicated in the data presented here is that for a fixed Strouhal number, there is a critical maximum angle of attack value beyond which the thrust coefficient will start to decrease and performance is reduced. A peak planform area thrust coefficient of 2.09 was measured at $h_{0.7}/c$=1.5, St=0.6 and α_{max}=30°. Increasing the heave-to-chord ratio from 1.5 to 2.0 does not appear to improve C_T values, but further iterations are still warranted. Combined with data from McLetchie (McLetchie, 2004), the data presented herein for the 3D foil suggests a useful performance trend where, for low α_{max}, high thrust and high efficiency can be gained at sufficiently high Strouhal numbers (St=0.6 and possibly higher). In particular, for higher roll amplitudes, these large oscillations produce high thrust with relatively little power loss. Higher thrust and efficiencies can be achieved through pre-shaping algorithms applied to the heaving/pitching foil motions for 2D flapping (Hover et al., 2004). Further investigation is warranted to determine whether pre-shaping would improve the performance of the 3D foil, but data suggests that this is a reasonable assumption.

Further comprehensive and systematic investigations of foil geometry on flapping foil performance are warranted; for example, it was suggested that an optimal aspect ratio is nearer to 4.0 for flapping wings (Polidoro, 2003). The effect of chordwise or spanwise flexibility on the performance of flapping foils is also still not well understood. Live fish employ active flexure of their fins, especially their pectoral fins, suggesting that they can optimize their fin shape for maximized performance (Fish and Lauder, 2006). Further experiments in tandem with numerical simulations are necessary to further augment our understanding of flapping foil performance as seen in nature.

List of symbols and abbreviations

c	foil chord
$\bar{c}$	mean chord
C_T	thrust coefficient
f	flapping frequency (Hz)
F_x, F_y, F_z	force components
$\bar{F}_{x_0}$	x-force component translated into reference frame of test section
$\dot{h}$	heave velocity ($\dot{h}$=dh/dt)
h_0	heave amplitude
$h_{0.7}$	heave amplitude at 0.7 span location
$h(t)$	heave position
M_x, M_y, M_z	moment components
r_0	radius from base of foil
$r_{0.7}$	radius from base of foil shaft to 0.7 span
P_{in}	power input
P_{out}	power output
Re	Reynolds number
S	foil span
St	Strouhal number
t	time
T	thrust
U	free stream velocity
α	angle of attack
α_{max}	maximum angle of attack
ψ	phase angle between pitch and roll
$\phi(t)$	roll angle
ϕ_0	roll amplitude
η	efficiency
μ	dynamic viscosity of the fluid (kg m^{-1} s^{-1})
ν	kinematic viscosity of the fluid [ν=μ/ρ (kg m^{-1} s^{-1})]
ρ	fluid density (kg m^{-3})
$\theta(t)$	pitch angle
θ_0	pitch amplitude
θ_{bias}	pitch bias angle
ω	circular frequency (rad s^{-1})

The author would like to thank K. Lim for his assistance with experiments and Dr Franz Hover for his insightful discussions related to data processing and angle of attack effects. The development of the flapping foil mechanism was made possible through the support of Admiral Paul Sullivan, NAVSEA, and the MIT Sea Grant program (Grant NA16RG2255).

References

Abbott, I. H. and Von Doenhoff, A. E. (1959). *Theory of Airfoil Sections*. New York: Dover Publications.
Anderson, J. M. (1996). Vorticity control for efficient propulsion. PhD thesis, MIT/Woods Hole Oceanographic Institution, USA.
Anderson, J. M. and Chabra, N. (2002). Maneuvering and stability performance of a robotoic tuna. *Integr. Comp. Biol.* **42**, 118-126.
Anderson, J., Streitlien, K., Barrett, D. and Triantafyllou, M. (1998). Oscillating foils of high propulsive efficiency. *J. Fluid Mech.* **360**, 41-72.
Bandyopadhyay, P. R. (2005). Trends in biorobotic autonomous undersea vehicles. *IEEE J. Oceanic Eng.* **30**, 109-139.
Bandyopadhyay, P. R., Castano, J. M., Rice, J. Q., Philips, R. B., Nedderman, W. H. and Macy, W. K. (1997). Low speed maneuvering hydrodynamics of fish and small underwater vehicles. *J. Fluids Eng.* **119**, 136-119.
Drucker, E. G. and Lauder, G. V. (1999). Locomotor forces on a swimming fish: three-dimensional vortex wake dynamics quantified using digital particle image velocimetry. *J. Exp. Biol.* **202**, 2393-2412.
Fish, F. and Hui, C. (1991). Dolphin swimming: a review. *Mammal Rev.* **21**, 181-195.
Fish, F. and Lauder, G. (2006). Passive and active flow control by swimming fishes and mammals. *Annu. Rev. Fluid Mech.* **38**, 193-224**.**
Flores, M. D. (2003). Flapping motion of a three-dimensional foil for propulsion and maneuvering of underwater vehicles. Masters thesis, MIT/Ocean Engineering, USA.
Freymouth, P. (1990). Thrust generation by an airfoil in hover modes. *Exp. Fluids* **9**, 17-24.
Hover, F. S., Haugsdal, O. and Triantafyllou, M. S. (2004). Effect of angle of attack profiles in flapping foil propulsion. *J. Fluids Struct.* **19**, 37-47.
Kato, N. (2000). Control performance of fish robot with mechanical pectoral fins in horizontal plane. *IEEE J. Oceanic Eng.* **25**, 121-129.
Katz, J. and Weihs, D. (1979). Large amplitude unsteady motion of a flexible slender propulsor. *J. Fluid Mech.* **90**, 713-723.
Koochesfahani, M. (1989). Vortical patterns in the wake of an oscillating foil. *AIAA J.* **27**, 1200-1205.
Lauder, G. V. (2000). Function of the caudal fin during locomotion in fishes: kinematics, flow visualization and evolutionary patterns. *Am. Zool.* **40**, 101-122.
Lim, K. L. (2005). Hydrodynamic performance and vortex shedding of a biologically inspired three-dimensional flapping foil. Masters Thesis, MIT/Ocean Engineering, USA.
Long, J. H., Schumacher, J., Livingston, N. and Kemp, M. (2006). Four flippers or two? Tetrapodal swimming with an aquatic robot. *Bioinspiration and Biomimetics* **1**, 20-29.
McLetchie, K. M. W. (2004). Forces and hydrodynamic efficiency measurements of a three dimensional flapping foil. Masters Thesis, MIT/Ocean Engineering, USA.
Polidoro, V. (2003). Flapping foil propulsion for cruising and hovering autonomous underwater vehicles. Masters Thesis, MIT/Ocean Engineering, USA.
Read, D. (2000). Oscillating foils for propulsion and maneuvering of ships and underwater vehicles. Masters thesis, MIT/Ocean Engineering, USA.
Read, D. A., Hover, F. S. and Triantafyllou, M. S. (2003). Forces on oscillating foils for propulsion and maneuvering. *J. Fluids Struct.* **17**, 163-183.
Triantafyllou, G. S., Triantafyllou, M. S. and Grosenbaugh, M. (1993). Optimal thrust development in oscillating foils with application to fish propulsion. *J. Fluids Struct.* **7**, 205-224.
Triantafyllou, M. and Triantafyllou, G. (1995). An efficient swimming machine. *Sci. Am.* **272**, 64-70.
Triantafyllou, M. S., Triantafyllou, G. S. and Yue, D. K. P. (2000). Hydrodynamics of fish-like swimming. *Annu. Rev. Fluid Mech.* **32**, 33-53.
Triantafyllou, M. S., Techet, A. H. and Hover, F. S. (2004). Review of experimental work in biomimetic foils. *IEEE J. Oceanic Eng.* **29**, 585-594.
Triantafyllou, M. S., Hover, F. S., Techet, A. H. and Yue, D. K. P. (2005). Review of hydrodynamic scaling laws in aquatic locomotion and fishlike swimming. *Appl. Mech. Rev.* **58**, 226-237.
Videler, J. (1993). *Fish Swimming*. London: Chapman & Hall.